(Received 11 December 2024, Accepted 3 March 2025, Scheduled 11 May 2025)

Modified IPD Expression for Radomes with Large Curvature

Pei Jia, Yongjun Xie, Chunyu Li, Ke Pang, Zhiping Li, Jiahui Zhao, and Peiyu Wu*

School of Electronic and Information Engineering, Beihang University, Beijing 100191, China

ABSTRACT: Primary insertion phase delay (IPD) expression is obtained using the flat plate model with plane wave incidence, and it only considers the longitudinal phase shift in the free space. This causes errors in large curvature radome applications since the longitudinal distance that wave travels in flat plate cannot represent the actual distance. Therefore, the IPD expression for radomes with large curvature should be defined. Based on the ray tracing in the radome medium, a modified IPD expression with more accurate transmission distance for large curvature radomes is proposed. The proposed expression can be applied to radomes with arbitrary curvature. The correctness of our proposed expression is verified via a simplified fast radome analytical model. The results from the proposed expression show errors within 1.0° for the parabolic radome system. The proposed expression can be applied to optimize the performance of radome systems with large curvature. A reflector antenna radome system is employed for verification. Results show that using the modified IPD expression to optimize the reflector antenna can increase the system gain by 1.8 dB, reduce the side lobe by 7.6 dB, and narrow the beamwidth by 0.9°.

1. INTRODUCTION

Radome is a functional component that protects the internal antenna from external environmental factors, such as wind, rain, and extreme temperatures. Radome plays a vital role in ensuring the reliable operation of various systems such as guidance, missile, communication, and telemetry systems [1–4]. Without a radome, these sensitive systems would be exposed to environmental degradation, leading to decreased performance and potentially catastrophic failure in mission-critical scenarios. However, while the radome provides essential protection, its presence introduces several challenges. One major drawback is insertion loss, where part of the signal power is lost as the electromagnetic wave passes through the radome material. Additionally, the radome can cause depolarization, altering the polarization state of the signal, which affects the quality and efficiency of signal transmission. Other damages, such as signal distortion and increased side-lobe levels, further compromise system performance. These effects can significantly degrade the functionality of the radome antenna system, especially in high-precision applications.

An important parameter to evaluate radome performance is the electrical thickness or the insertion phase delay (IPD) of the radome. The IPD reflects the phase distortion of the electromagnetic wave as it passes through the radome material and is critical in determining how the radome impacts signal transmission [5–8]. Accurately analyzing and calculating the IPD of a radome is of significant value to the performance and design of the radome system [9–12].

IPD is defined as the phase delay introduced by the presence of the wall relative to free-space conditions [13, 14]. It is influenced by various factors, and there are several expressions for calculating IPD in the published literature. The phase of the transmission coefficient is directly regarded as IPD in some literature [13, 15]. This expression is not consistent with the definition of IPD because it does not consider the phase delay in the free space. The IPD expression considering the free space phase delay can be used to evaluate the radome electrical performance [16–18]. It can be expressed as

$$IPD_{\perp/\parallel} = \angle T_{\perp/\parallel} - k_0 d \cos\theta_{\mathrm{i}} \tag{1}$$

where $\perp$ and $\parallel$ denote the vertical and horizontal polarizations, respectively; $\angle T$ is the phase of the transmission coefficient T; k_0 is the propagation constant in the free space; d is the thickness of the radome; and θ_i is the incidence angle. Some literatures derive the simplified IPD expression based on (1) under certain conditions. The IPD expression that neglects multiple reflections of the wave inside the medium can be used to locate the radome defects [19] and to estimate the radome thickness [20]. The approximate expression of IPD for the very thin slab can be used to estimate the dielectric constant of the medium accordingly [21]. The unsimplified and simplified expressions cause errors when IPD is analyzed for radomes with large curvature, because the d in the subtracted term in (1) is the thickness of the dielectric and is obtained using the flat plate equivalent model. It cannot present the actual wave transmission distance in curve dielectrics. Therefore, it is necessary to propose more precise IPD expression for radomes with large curvature.

Here, a modified IPD expression applying more accurate transmission distance is proposed for radomes with large curvature. A two-dimensional simplified radome model and a three-dimensional reflector antenna radome system are employed for verification. Results show that the modified expression can ensure the IPD calculation accuracy for radomes with large curvature and be applied to system performance improvement.

* Corresponding author: Peiyu Wu (wupuuu@yahoo.com).

2. THEORETICAL DEMONSTRATION

IPD is important in performance evaluation of radomes. In this paper, we mainly consider IPD expression for single-layer applications since multilayer applications can be derived from the single-layer case as follows [22–24]

$$IPD = \angle T' - k_0 d' \cos\theta_{\rm i}. \tag{2}$$

Here, $\angle T'$ is the phase angle of the transmission coefficients for the multilayer dielectric, and d' is the total thickness of the multilayer dielectric.

Theoretically, IPD is expected to be negative. The value of (1) only represents the delay without indicating positive or negative. To align the definition of IPD with the results from the theoretical expression, certain adjustments are applied to the calculation expression, expressed as follows

$$\begin{aligned} IPD &= -(\angle T - k_0 d\cos\theta_{\rm i}) \\ &= -\angle T + k_0 d\cos\theta_{\rm i}. \end{aligned} \tag{3}$$

$$IPD' = \begin{cases} IPD - 360, & if \quad IPD \geq 0 \\ IPD, & if \quad IPD < 0 \end{cases}. \tag{4}$$

2.1. Phase Delay in the Dielectric

As shown in Fig. 1, there are two kinds of complex transmission coefficient T_C and T_M [25]. According to the $ABCD$ transmission matrix, the more accurate complex transmission coefficient considering the lateral transmission phase shift for the single-layer dielectric radome can be written as ([25])

$$\begin{aligned} T_M &= \frac{2e^{-jk_0\sin\theta_i d\tan\theta_t}}{2\cos(vd\cos\theta_t) + j\left(N+\frac{1}{N}\right)\sin(vd\cos\theta_t)} \\ &= |T_M|\, e^{-j\angle T_M} \end{aligned} \tag{5}$$

where

$$v = k_0\sin\theta_i / \sin\theta_t \tag{6}$$

$$N = \begin{cases} \frac{Z_1\cos\theta_i}{Z_0\cos\theta_t} = \frac{\cos\theta_i}{\sqrt{\varepsilon_r - \sin^2\theta_t}}, & \text{vertical polarization} \\ \frac{Z_1\cos\theta_t}{Z_0\cos\theta_i} = \frac{\sqrt{\varepsilon_r - \sin^2\theta_i}}{\varepsilon_r\cos\theta_i}, & \text{horizontal polarization} \end{cases}. \tag{7}$$

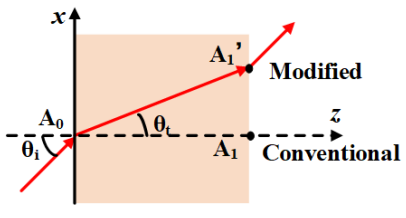

FIGURE 1. Propagation model in dielectric plane.

The primary one without considering the lateral transmission phase shift A_1A_1' can be expressed as

$$T_C = |T_M|\, e^{-j\phi_{T_M}} e^{jk_0\sin\theta_i d\tan\theta_t} = |T_C|\, e^{-j\phi_{T_C}}. \tag{8}$$

In (8), we analyze the difference between T_C and T_M for single-layer dielectric according to ([25]). Using different transmission coefficients can cause large difference in the IPD values. We use the modified transmission coefficient T_M to derive IPD, since when the wave is not normal incidence to the radome, the lateral phase delay A_1A_1' due to refraction cannot be ignored.

2.2. Phase Delay in the Free Space

It can be observed from Fig. 2(a) that the departure point of the wave at the medium's outer wall when using the flat plate equivalent is at A. And the phase delay in free space $k_0 d\cos\theta_{\rm i}$ in (3) only removes the corresponding vertical phase shift d_1 in the free space.

However, as shown in Fig. 2(b), by tracing the ray in the free space, it is clear that the main route of wave passing through the free space is d_2. The lateral and longitudinal phase shifts caused by d_2 can be expressed as

$$\begin{cases} \varphi_x = k_{0x} d_{B'A'} = k_0\sin\theta_i d_{B'A'} \\ \varphi_y = k_{0y} d_{O'B'} = k_0\cos\theta_i d_{O'B'} \end{cases}. \tag{9}$$

Then the phase shift caused by d_2 is

$$\vec{k}_0 \cdot \vec{d}_2 = k_{0y} d_{O'B'} + k_{0x} d_{A'B'} = \varphi_y + \varphi_x. \tag{10}$$

As shown in Fig. 2(b), the wave propagating to A' through dielectrics intersects the front surface at O. There is a phase advance between O' and O when the wave passes through in free space. It can be expressed as

$$\varphi_a = k_{0x} d_{O'O} = k_0\sin\theta_i d_{O'O}. \tag{11}$$

To calculate the IPD more exactly, the total phase delay in free space needs to incorporate the phase delay caused by d_2 and the phase advance φ_a. Thus, the total modified phase delay in free space is

$$\begin{aligned} \varphi_d &= \varphi_x + \varphi_y - \varphi_a \\ &= k_{0x} d_{B'A'} + k_{0y} d_{O'B'} - k_{0x} d_{O'O} \\ &= k_{0x} d_{BA'} + k_{0y} d_{O'B'} \\ &= k_0\sin\theta_i d_{BA'} + k_0\cos\theta_i d_{O'B'} \end{aligned} \tag{12}$$

where $d_{BA'}$ and $d_{O'B'}$ are

$$d_{BA'} = d_{OA'}\sin\theta_t \tag{13}$$

$$d_{O'B'} = d_{OB} = d_{OA'}\cos\theta_t. \tag{14}$$

Here, θ_t is the refraction angle in the dielectric, and $d_{OA'}$ is a more accurate transmission shift which can be calculated by ray tracing in the dielectric.

Then, the modified IPD expression with a more accurate transmission distance can be expressed as

$$\begin{aligned} &IPD_{\perp/\parallel} \\ &= -(\angle T_{M\perp/\parallel} - \varphi_d) \\ &= -\angle T_{M\perp/\parallel} + k_0\sin\theta_i d_{BA'} + k_0\cos\theta_i d_{O'B'} \\ &= -\angle T_{M\perp/\parallel} + k_0\sin\theta_i d_{OA'}\sin\theta_t + k_0\cos\theta_i d_{OA'}\cos\theta_t. \end{aligned} \tag{15}$$

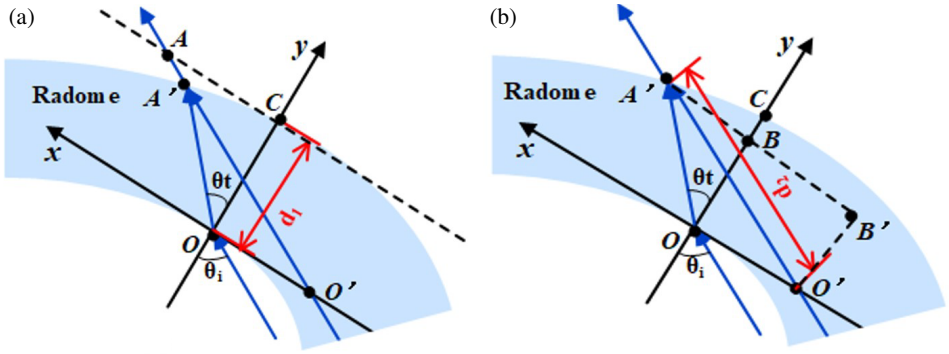

FIGURE 2. Propagation model in the curved radome. (a) The primary model obtained from the flat plate equivalent model and (b) the modified model obtained from ray tracing method.

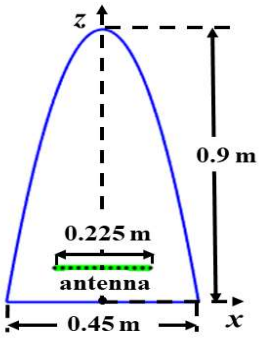

FIGURE 3. The system sketch of the parabolic radome system.

3. VERIFICATION WITH RADOME SYSTEM

In order to demonstrate the effectiveness of the proposed modified IPD expression, the difference between primary IPD and modified IPD expressions is quickly analyzed through a simplified two-dimensional radome analysis model based on physical optics (PO) method. The calculation was done by a Matlab program. Antenna system and its radome have 3D geometry, but 2D radome systems with simple nonvectorial nature can still be used in modeling and analyzing [26, 27]. We focus solely on vertical polarization, as the parallel polarization case is similar to the vertical polarization case.

According to the PO method, when the radome is present, the inner surface field of the radome can be obtained by summing the field vectors radiated by the antennas inner field E_i and H_i. Then, the tangential electromagnetic field at the outer wall of the radome is [28]

$$\vec{E}_t = \left[\left(\hat{v}\cdot\vec{E}_i\right)\hat{v}\right]T_{\perp} \tag{16}$$

$$\vec{H}_t = \left[\left(\hat{h}\cdot\vec{H}_i\right)\hat{h}\right]T_{//} \tag{17}$$

where $\hat{v}$ and $\hat{h}$ represent unit tangential vectors perpendicular and parallel to the incident plane of the radome, respectively.

When the radome is absent, the field at radome outer wall is obtained by summing the field vectors radiated by the antennas. Then, according to the definition in [20], the simulation results of the IPD are obtained by the phase difference between the positions in the radome outer surface in the presence and absence of the radome.

Figure 3 shows the system sketch of a parabolic radome system. The radome has a fineness ratio of 2. The base diameter and the height of the radome are 0.45 and 0.90 m, respectively. The antennas are represented by current sources extending indefinitely in the y-direction, evenly spaced along the x-axis. The current sources operate at 8 GHz and are located at a distance of 0.11 m from the radome base. This distance can provide certain degrees of freedom for array rotation. The inter-element spacing of the array is about 18.75 mm, which is half the distance of the wavelength. The array consists of 13 elements with a distribution range about half of the radome's base diameter, so that the main radiating area of the antenna can cover the center of the radome. The relative permittivity and loss tangent are 2.33 and 0.015, respectively. Here, the primary radiation region of the antenna on the radome is discussed, corresponding to the theta varying from $-10°$ to $10°$.

As shown in Fig. 4, the primary IPD expression (3) with T_M agrees with the simulated IPD only when the wave is almost normally insistent. When the radome curvature is smaller than 3.2, both the primary IPD expression (3) with T_C and the modified IPD expression agree well with the simulated IPD values. However, when the curvature is larger than 3.2, only the results

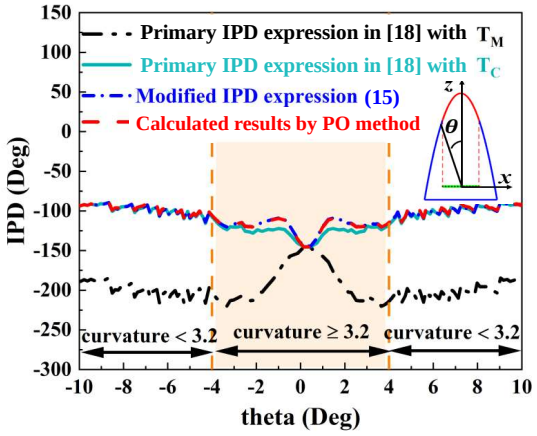

FIGURE 4. Curvature and IPD distribution of the simplified parabolic radome system calculated from different approaches.

calculated by the modified IPD expression can agree well with the simulated values.

It can also be observed that using different transmission coefficients for radomes with large curvature can cause large difference. The primary IPD expression with T_C, instead of causing greater deviation, gives less deviation than the primary IPD expression with T_M. This is because both the T_C and phase delay in the free space, as used in the primary expression, fail to account for the lateral phase shift. When these inaccurate terms are subtracted from each other, their errors partially offset, resulting in a deceptively smaller error in the IPD. This result shows that the primary IPD expression with T_C is not sensitive to the lateral phase shift caused by oblique incidence. However, it should be noticed that T_M is a more accurate expression and can better describe the wave propagation in the dielectric according to [25]. Therefore, our proposed IPD expression is derived using the modified transmission coefficient T_M, and the modified and primary expressions with T_M are mainly compared in the subsequent study.

As shown in Table 1, when the radome curvature is smaller than 3.2 and the curvature radius greater than approximately 8 times of the wavelength, the average IPD error of the proposed expression (15) is within $1.0°$; when the radome curvature is larger than 3.2 and the curvature radius smaller than approximately 8 times of the wavelength, the average IPD error of the proposed expression (15) is within $0.4°$, which is significantly lower than the average error of the primary IPD expressions.

According to the above analysis, the usage conditions of the primary and modified IPD expressions are summarized and presented in Table 2.

4. MODIFIED IPD EXPRESSION APPLICATION IN REFLECTOR SHAPING

To verify the practicality of the proposed expression, we apply it to reflector antenna shaping optimization in the radome system [11, 12]. The optimization effect is evaluated by HFSS, and the comparison between the proposed expression and primary IPD expression is performed.

The aperture field of an ideal reflector antenna maintains an equal-phase surface, and it will be distorted due to the existence of radome. This distortion can be reduced by compensating the negative value of IPD to the antenna aperture field, so that the aperture field can become equiphase again after transmitting through the radome.

Since both the radome and reflector surface exhibit rotational symmetry, the phase distortion of the antenna aperture also exhibits rotational symmetry. Therefore, only the reflector antenna generatrix needs to be shaped according to the IPD distribution along the generatrix.

Figure 5 shows the system sketch of a reflector antenna radome system. The center frequency of the metal reflector antenna is 22 GHz, and the wavelength is 13.6 mm. The focal length of the reflector is 0.341 m. The size of the metal reflector is $D_0 = 0.491$ m, and the feed is a horn antenna. The base diameter and the height of the radome are 0.675 and 0.899 m, respectively. The radome material is polytetrafluoroethylene

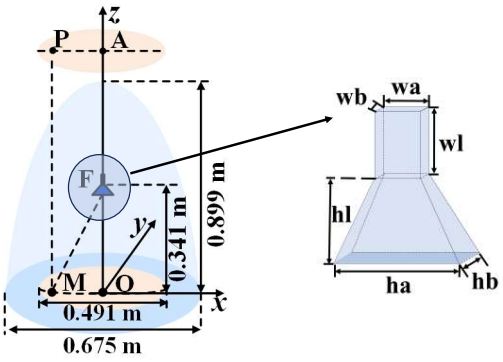

FIGURE 5. The system sketch of the reflector antenna radome system.

(PTFE), the relative permittivity and loss tangent are 2.33 and 0.015, respectively. The parameters of the metal horn antenna are shown in Table 3.

The location of point M on the reflector generatrix can be represented using IPD as [12]

$$z_M = \frac{{x_M}^2 - 2Qf - Q^2}{4f + 2Q} \tag{18}$$

where

$$Q = \frac{IPD(A) - IPD(P)}{k_0}. \tag{19}$$

Here, $IPD(A)$ and $IPD(P)$ are the IPD at A and P, respectively, as shown in Fig. 5.

Figure 6 shows the results of the reflector shaping using different IPD expressions. It can be obtained that the reflector generatrix obtained from the modified IPD has a intermediate degree of inclination in the end area of the reflector.

The generatrixs are fitted based on the calculated discrete points using fifth-order polynomial. Their fitting errors are less than 1×10^{-5}, which are negligible.

Figure 7 shows the comparisons of system far-field pattern optimized using the proposed IPD expression (15) with that using the primary IPD expression (3), and the corresponding

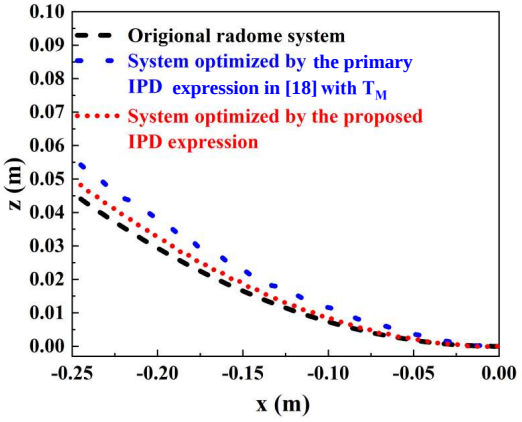

FIGURE 6. Original reflector generatrix and optimized reflector generatrix calculated from different IPD expressions.

TABLE 1. Average IPD error for parabolic radome system.

Regions		Primary IPD expression in [18] with T_C	Primary IPD expression in [18] with T_M	This work
Curvature	Curvature radius /wavelength			
$\leqslant 3.2$	$\geqslant 8.3$	1.5°	102.0°	1.0°
>3.2	<8.3	6.6°	76.9°	0.4°
$\leqslant 3.2$	$\geqslant 8.3$	1.5°	102.0°	1.0°

TABLE 2. Usage conditions of the three IPD expressions.

IPD Expression	Curvature radius / wavelength	Incident angle
Primary IPD expression in [18] with T_C	Applicable when the curvature radius exceeds 8 times the wavelength.	Accuracy is insensitive to the incident angle.
Primary IPD expression in [18] with T_M	Accuracy is insensitive to the ratio of curvature radius and wavelength.	Applicable for normal incidence.
Modified IPD expression (15)	Applicable for any curvature radius and wavelength.	Accuracy is insensitive to the incident angle.

TABLE 3. Parameters of the horn antenna.

Horn Structure	Length (mm)	Horn Structure	Length (mm)
Waveguide_a (wa)	0.711 λ	Horn_a (wa)	3.018 λ
Waveguide_a (wb)	0.355 λ	Horn_b (wb)	2.349 λ
Waveguide_length (wl)	1.657 λ	Horn_l (wl)	2.524 λ

TABLE 4. Compensation effect of radome system.

22GHz		AR	SAWR using primary IPD in [18] with T_M	SAWR using modified IPD
Maximum Directivity (dB)	E-plane	31.0	33.6	32.8
	H-plane	31.0	33.6	32.8
Sidelobe (dB)	E-plane	-18.7	-14.4	-18.3
	H-plane	-15.0	-17.7	-22.6
3dB beamwidth (deg)	E-plane	4.1	3.2	3.2
	H-plane	3.3	2.7	2.6

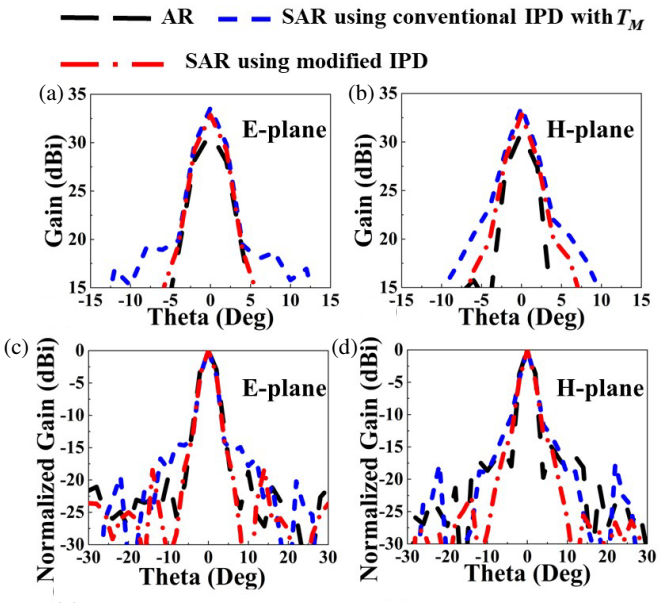

FIGURE 7. Simulated radiation patterns of the radome systems optimized by different IPD expression: antenna with radome(AR); shaped antenna with radome(SAWR). (a) system gain in E-plane (b) system gain in H-plane (c) system normalized gain in E-plane (d) system normalized gain in H-plane.

performances are given in Table 4. Higher gain and narrower 3 dB beamwidth can be observed from the shaped antenna with radome (SAWR) system obtained from both modified and primary IPD expressions. However, only the SAWR system obtained from modified IPD expression can exhibit better performance in the sidelobe lever. After applying the modified IPD expression, the maximum directivity of the SAWR system can be increased by 1.8 dB, the sidelobe reduced by 7.6 dB, and the beamwidth narrowed by $0.9°$ compared with the original antenna with radome (AR) system.

5. CONCLUSION

Modified IPD expression for radomes with large curvature is proposed by tracing rays of the wave. The modified expression is verified via a simplified fast radome analytical model, and it can be applied to reflector shaping. Conclusions are drawn as follows:

1) The modified expression employs a more accurate transmission distance in the radomes. This enables the modified expression to be applied to the accurate calculation of IPD system performance improvement for radomes with large curvature. The simulation results demonstrate that the modified expression provides a more accurate evaluation of the large curvature radome IPD, with the error within $1.0°$ in the parabolic radome system.

2) Using the modified IPD expression to shape the reflector antenna can get an overall better system performance than using the primary IPD expression for radomes with large curvature. Simulation results show that the system gain increases 1.8 dB; the sidelobe decreases 7.6 dB; and the 3 dB beamwidth narrows $0.9°$. The reported findings are believed to provide guidelines for curved radomes performance analysis and optimization. Further attention may be paid to the limitations of the large-size reflector radome systems such as complex reflector generatrix and accompanied manufacturing difficulties.

ACKNOWLEDGEMENT

This work was supported by the Beijing Natural Science Foundation (4242005), National Natural Science Foundation of China (62301013, 61971022), National Key Laboratory of Science and Technology on Space Microwave (6142411032201) and National Key Research and Development Program of China (2020YFB1807400).

REFERENCES

[1] Wang, S., H.-X. Xu, M. Wang, H. Wei, F. Zhang, and G. Hu, "Janus metasurface for super radome with asymmetric diffusion and absorption," *Advanced Optical Materials*, Vol. 12, No. 7, 2302061, 2024.

[2] Yang, J., H. Zheng, Y. Pang, B. Qu, Y. Li, J. Wang, and Z. Xu, "Design, modelling, and manufacturing of sandwich radome structure with out-of-band absorption and in-band transmission performances," *Composite Structures*, Vol. 339, 118138, 2024.

[3] Haider, I., I. H. Gul, S. Aziz, M. I. Faraz, M. A. Khan, S. H. I. Jaffery, and D.-W. Jung, "Environmental aging of reinforced polymer composite radome: Reliability and performance investigation," *Frontiers in Materials*, Vol. 11, 1427541, 2024.

[4] Wang, B., B. Luo, Q. Yan, Y. Yang, W. Bao, Z. Qiu, H. Fan, and J. Dai, "Effects of lattice configuration on multifunctionality of C-sandwich radome," *International Journal of Mechanical Sciences*, Vol. 267, 108972, 2024.

[5] Joy, V., A. J. Teena, H. Singh, and R. Nair, "Optimal design methodology for planar multi-layered radomes for multiband applications using nature inspired algorithm," *Progress In Electromagnetics Research C*, Vol. 106, 121–136, 2020.

[6] Duan, W., J. Xie, M. Bi, L. Qi, Y. Li, K. Li, Z. Li, and X. Weng, "Study on the electromagnetic performance of radome with laminar ablation for reentry applications," *IEEE Transactions on Antennas and Propagation*, Vol. 72, No. 8, 6261–6269, 2024.

[7] Duan, W., X. Weng, Y. Li, Z. Li, S. Bao, and M. Bi, "Temperature-dependent electromagnetic performance predictions of a hypersonic radome based on variable thickness gradient dielectric multilayer walls," *IEEE Antennas and Wireless Propagation Letters*, Vol. 23, No. 8, 2381–2385, 2024.

[8] Duan, W., X. Weng, Y. Li, Z. Li, S. Bao, and M. Bi, "Temperature-dependent electromagnetic performance predictions of a hypersonic radome based on variable thickness gradient dielectric multilayer walls," *IEEE Antennas and Wireless Propagation Letters*, Vol. 23, No. 8, 2381–2385, 2024.

[9] Ji, J., J. Ren, X. Jiang, W. Wang, H. Yu, K. Yin, and B. Chen, "A novel method for calculating broadband electrical performance of high-speed aircraft radome under thermo-mechanical-electrical coupling," *Chinese Journal of Aeronautics*, Vol. 37, No. 9, 463–474, 2024.

[10] Arya, K. M., A. M. Aserkar, S. A. Patil, R. Nair, and S. Narayan, "Design of multiband metasurface radome for leading wing edge of aircraft," *Progress In Electromagnetics Research M*, Vol. 130, 37–48, 2024.

[11] Li, P., W. Y. Xu, and L. W. Song, "A novel compensation strategy for the radiation characteristics of large dielectric radomes based on phase modification," *IEEE Antennas and Wireless Propagation Letters*, Vol. 15, 1044–1047, 2015.

[12] Xu, W., B. Duan, P. Li, Y. Zong, and Y. Qiu, "Novel compensation method for electromagnetic performance of dielectric radome based on reflector shaping," *IET Microwaves, Antennas & Propagation*, Vol. 9, No. 2, 125–132, 2015.

[13] Kedar, A., K. Beenamole, and U. Revankar, "Performance appraisal of active phased array antenna in presence of a multilayer flat sandwich radome," *Progress In Electromagnetics Research*, Vol. 66, 157–171, 2006.

[14] Liu, Z., X. Fan, J. Zhang, L. Chen, Y. Tang, J. Kong, and J. Gu, "PBO fibers/fluorine-containing liquid crystal compound modified cyanate ester wave-transparent laminated composites with excellent mechanical and flame retardance properties," *Journal of Materials Science & Technology*, Vol. 152, 16–29, 2023.

[15] Kedar, A. and U. Revankar, "Parametric study of flat sandwich multilayer radome," *Progress In Electromagnetics Research*, Vol. 66, 253–265, 2006.

[16] Li, P., W. Pedrycz, W. Xu, and L. Song, "Far-field pattern tolerance analysis of the antenna-radome system with the material thickness error: An interval arithmetic approach," *IEEE Transactions on Antennas and Propagation*, Vol. 65, No. 4, 1934–1946, 2017.

[17] Ji, J., W. Wang, H. Yu, J. Liu, and B. Chen, "Investigation of the electrical performance of high-speed aircraft radomes using a thermo-mechanical-electrical coupling model," *Journal of Systems Engineering and Electronics*, Vol. 35, No. 6, 1397–1410, 2024.

[18] Shin, H., D. Yoon, D.-Y. Na, and Y. B. Park, "Analysis of transmission loss and boresight error of a curved FSS radome-enclosed antenna," *IEEE Access*, Vol. 9, 95 843–95 852, 2021.

[19] Persson, K., M. Gustafsson, and G. Kristensson, "Reconstruction and visualization of equivalent currents on a radome using an integral representation formulation," *Progress In Electromagnetics Research B*, Vol. 20, 65–90, 2010.

[20] Persson, K., M. Gustafsson, G. Kristensson, and B. Widenberg, "Radome diagnostics — Source reconstruction of phase objects with an equivalent currents approach," *IEEE Transactions on Antennas and Propagation*, Vol. 62, No. 4, 2041–2051, 2014.

[21] Mahony, J. D., "Measurements to estimate the relative permittivity and loss tangent of thin, low-loss materials," *IEEE Antennas and Propagation Magazine*, Vol. 47, No. 3, 83–87, 2005.

[22] Liang, D., H. Li, Y. Fu, and X. Pang, "A novel transmission loss compensation method for radome based on non-linear frequency modulation waveform design," *Electronics Letters*, Vol. 59, No. 14, e12876, 2023.

[23] Mohammed Yazeen, P. S., C. V. Vinisha, S. Vandana, M. Suprava, and R. U. Nair, *Broadbanding Techniques for Radomes*, Springer, 2020.

[24] Arya, K. M., A. M. Aserkar, S. A. Patil, R. Nair, and S. Narayan, "Design of multiband metasurface radome for leading wing edge of aircraft," *Progress In Electromagnetics Research M*, Vol. 130, 37–48, 2024.

[25] Meng, H., W. Dou, T. Chen, and K. Yin, "Analysis of radome using aperture integration-surface integration method with modified transmission coefficient," *Journal of Infrared, Millimeter, and Terahertz Waves*, Vol. 30, 199–210, 2009.

[26] Oğuzer, T. and A. Altintas, "Analysis of the nonconcentric radome-enclosed cylindrical reflector antenna system, E-polarization case," *Journal of Electromagnetic Waves and Applications*, Vol. 19, No. 15, 2093–2111, 2005.

[27] Chen, H., Z. Shen, and E. Li, "Analysis of a three-dimensional antenna radiating through a two-dimensional radome using a fast high-order method," *IEEE Transactions on Magnetics*, Vol. 42, No. 4, 699–702, 2006.

[28] Fan, X. and Q. Zhang, "Optimization of two-dimensional radome boresight error performance based on GA," *Modern Electronics Technique*, Vol. 34, 9–11, 2011.